



# CHORUS

This is the accepted manuscript made available via CHORUS. The article has been published as:

## Electric field control of the Verwey transition and induced magnetoelectric effect in magnetite

Jared J. I. Wong, Adrian G. Swartz, Renjing Zheng, Wei Han, and Roland K. Kawakami

Phys. Rev. B **86**, 060409 — Published 24 August 2012

DOI: [10.1103/PhysRevB.86.060409](https://doi.org/10.1103/PhysRevB.86.060409)

# Electric Field Control of the Verwey Transition and Induced Magnetoelectric Effect in Magnetite

Jared J. I. Wong, Adrian G. Swartz, Renjing Zheng, Wei Han, and Roland K. Kawakami\*

*Department of Physics and Astronomy,  
University of California, Riverside, CA 92521, USA*

## Abstract

We incorporate single crystal  $\text{Fe}_3\text{O}_4$  thin films into a gated device structure and demonstrate the ability to control the Verwey transition with static electric fields. The Verwey transition temperature ( $T_V$ ) increases for both polarities of the electric field, indicating the effect is not driven by changes in carrier concentration. Energetics of induced electric polarization and/or strain within the  $\text{Fe}_3\text{O}_4$  film provide a possible explanation for this behavior. Electric field control of the Verwey transition leads directly to a large magnetoelectric effect with coefficient of 585 pT m/V.

PACS numbers: 75.47.Lx, 71.27.+a, 75.85.+t, 71.30.+h

Electric field control of magnetic and metal-to-insulator transitions in highly correlated materials has generated great interest both scientifically and technologically [1–5]. Magnetite ( $\text{Fe}_3\text{O}_4$ ) is a highly correlated material that undergoes the well-known Verwey transition with sharp changes in the electric, magnetic, and structural properties at a transition temperature of  $T_V \sim 120$  K [6–8]. The Verwey transition, discovered in 1939 as one of the first metal-to-insulator transitions generated by electron-electron correlations, has been studied intensively over the past seven decades. Theoretically, Verwey proposed that the transition is due to charge ordering below  $T_V$  and subsequent models based on Mott insulator theory and band theory emerged [8]. Experimentally, studies on bulk single-crystals have established that stoichiometry, impurities, and hydrostatic pressure (strain) are important factors in determining  $T_V$  [6–9]. Interestingly, the original hypothesis of charge ordering was verified only within the past few years by x-ray scattering [10–16]. Magnetite is also ferroelectric at low temperatures ( $<38$  K) having an unusual case of ferroelectricity that originates from charge ordering of the  $\text{Fe}^{2+}$  and  $\text{Fe}^{3+}$  ions [17–21]. The electrical polarization in magnetite is generated by the rearrangement of electron distribution without a large corresponding displacement of lattice atoms [18]. Furthermore, this ferroelectric state exhibits a magnetoelectric effect where electrical polarization can be tuned by the orientation of a static magnetic field in relation to a poled perpendicular electric field [19, 21]. More recently, theoretical predictions of half-metallic behavior (100% spin polarization) [22] have motivated studies of magnetite thin films and heterostructures including incorporation into magnetic tunnel junctions [23] and integration with semiconductors [24]. Studies of thin films show the Verwey transition is weakened at low film thickness and the charge-ordered Verwey state can be destroyed by high current densities [3, 25]. Due to these interesting properties, magnetite has been the subject of many investigations by researchers in correlated electron materials, multiferroics, and spintronics.

In this Letter, we demonstrate that static electric fields can control the Verwey transition in  $\text{Fe}_3\text{O}_4$  thin films. Our experiments utilize an electrostatic gate to apply a static electric field to a 50 nm magnetite film. It is found that the application of either positive or negative electric fields leads to an increase of the transition temperature ( $T_V$ ). This result is quite surprising and intriguing because it was theoretically unpredicted despite years of intense research with magnetite and on the Verwey transition. Furthermore, electric field control of  $T_V$  leads to a new mechanism for generating a magnetoelectric effect distinct

from the traditional magnetoelectric effect in ferroelectric magnetite [19, 21]. Previous demonstrations of electric field control of magnetic and metal-to-insulator transitions have resulted from various effects including current-induced breakdown of the insulating state [2, 3, 26], field-induced changes of carrier concentration [4, 27], field-induced strain generated by growth on piezoelectric substrate (i.e. composite system) [5, 28–30]. The results reported here are significantly distinct from these previous categories. Particularly, while current-induced breakdown is a highly non-equilibrium process, the present effect produces a true change in the equilibrium phase transition. We also find that this effect is not due to changes in carrier concentration, as shown by a symmetric dependence of  $T_V$  on gate voltage. Finally, this effect does not rely on external strain provided by adjacent layers. Thus, the electric field control of the Verwey transition represents a new type of electric field control in a highly correlated material.

$\text{Fe}_3\text{O}_4$  films of 50 nm thickness are grown on double-side polished  $\text{MgO}(001)$  substrates using reactive molecular beam epitaxy (MBE) in ultrahigh vacuum (UHV) with a base pressure of  $1 \times 10^{-10}$  torr.  $\text{MgO}$  substrates are first rinsed with de-ionized (DI) water. After loading into the MBE chamber, substrates are annealed at  $600^\circ\text{C}$  for 45 minutes. A 10 nm  $\text{MgO}$  buffer layer is grown at  $350^\circ\text{C}$  via electron beam (e-beam) deposition from an  $\text{MgO}$  source [31]. Next, the  $\text{Fe}_3\text{O}_4$  layer is grown at  $200^\circ\text{C}$  by depositing elemental Fe in a molecular oxygen partial pressure of  $1.2 \times 10^{-7}$  torr. The Fe is evaporated from a thermal effusion cell at a rate of  $\sim 0.13$  nm/min (for pure Fe). The single-crystal structure is verified through *in situ* reflection high energy electron diffraction (RHEED) and low energy electron diffraction (LEED), as shown in Figs. 1a, 1b, and 1c inset.  $\theta - 2\theta$  high resolution x-ray diffraction (HRXRD) scans exhibit a  $\text{Fe}_3\text{O}_4(004)$  peak near the  $\text{MgO}(002)$  substrate peak (Fig. 1c). Kiessig interference fringes indicate atomically smooth interfaces and verify the film thickness.

Electrical properties of  $\text{Fe}_3\text{O}_4$  films are characterized using standard dc four-point probe measurements (Figure 1d inset). Resistance values are obtained from current-voltage ( $I$ - $V$ ) curves, which exhibit linear dependence (Figure 1e) above 70 K. The temperature dependence of resistance (Figure 1d, blue) exhibits a metal-to-insulator transition with a substantially higher resistance below 117 K, indicating the Verwey transition. Temperature dependence curves are measured as a function of increasing temperature, with the temperature stabilized for 10 min before a measurement is taken. For each temperature, measurements

are repeated to ensure the temperature is stable.

The magneto-optic Kerr effect (MOKE), with laser beam incident through the transparent MgO substrate, is used to characterize the magnetic properties of the  $\text{Fe}_3\text{O}_4$  films (812 nm wavelength,  $p$ -polarized,  $45^\circ$  angle of incidence). Figure 1f shows a typical longitudinal MOKE hysteresis loop that exhibits large remanence and sharp magnetization reversal. The right hand axis of Fig. 1f displays the corresponding magnitude of the magnetization based on superconducting quantum interference device (SQUID) magnetometry. The temperature dependence of the MOKE signal (Figure 1d, red) exhibits a decrease of magnetization for temperatures below  $T_V$ . This behavior is characteristic of the Verwey transition in thin films, which is typically less sharp than in bulk materials.

To apply electric fields to the  $\text{Fe}_3\text{O}_4$  film, an insulating layer (PMMA/ $\text{Al}_2\text{O}_3$ /MgO) is deposited on top of the  $\text{Fe}_3\text{O}_4$ , followed by a metallic electrostatic gate (Pd/Ti), as shown schematically in Figure 2a. The devices are fabricated through several steps of evaporation using shadow masks. For the  $\text{Fe}_3\text{O}_4$  layer, a narrow channel is produced with a width of  $210 \mu\text{m}$ , creating a small active area to reduce the occurrence of pinholes and gate leakage. The  $\text{Fe}_3\text{O}_4$  channel length is 4.2 mm and the gate length is 3.3 mm. Alternate samples with  $\text{Fe}_3\text{O}_4$  films covering a large area of the substrate produce similar results [32]. Pd(100 nm)/Ti(15 nm) contacts (for four-point probe) are e-beam evaporated through a shadow mask in a separate system. Then a 10 nm MgO layer is grown on the  $\text{Fe}_3\text{O}_4$  followed by a 50 nm  $\text{Al}_2\text{O}_3$  layer. PMMA is then spin coated onto the sample at 3000 rpm and cured under a vacuum environment at  $170^\circ\text{C}$ . The spin coating and baking sequence is repeated three times giving a final PMMA layer thickness of 900 nm. Finally, a shadow mask is used to grow the Pd(100 nm)/Ti(15 nm) top gate electrode. Typical gate leakage is 0.5 nA for electric fields of  $\pm 1.8 \text{ MV/cm}$ .

An electric field is produced by applying a voltage ( $V_G$ ) between the gate electrode and the  $\text{Fe}_3\text{O}_4$  film. Figure 2b shows the temperature dependence of resistance for applied electric fields of  $+1.8 \text{ MV/cm}$  ( $V_G = +60 \text{ V}$ , blue),  $+0.9 \text{ MV/cm}$  ( $V_G = +30 \text{ V}$ , orange),  $0 \text{ MV/cm}$  ( $V_G = 0 \text{ V}$  black),  $-0.9 \text{ MV/cm}$  ( $V_G = -30 \text{ V}$ , green),  $-1.8 \text{ MV/cm}$  ( $V_G = -60 \text{ V}$ , red) with corresponding colored arrows indicating  $T_V$ . The data clearly show that  $T_V$  varies as a function electric field, as summarized in the inset of Fig. 2c. At zero electric field,  $T_V$  is 117 K. Strikingly, both positive and negative electric fields cause  $T_V$  to increase, indicating that the shift in  $T_V$  depends primarily on the magnitude of electric field as opposed to its sign.

The maximum effect is observed for -1.8 MV/cm, where  $T_V$  increases to 119 K, giving  $\Delta T_V = +2$  K. At a similar electric field, the largest  $\Delta T_V$  we observe in our study is  $\Delta T_V = +6$  K for a large area sample [32]. The increase of  $T_V$  cannot be due to Joule heating because a heating artifact would appear as a reduction of  $T_V$ . We also rule out effects of irreversible sample change by measuring the zero electric field temperature dependence of resistance before and after taking the data in Fig. 2b and no irreversible changes were observed. Finally, we observe that temperature dependent resistance above  $T_V$  does not change with applied electric field, which shows that the metallic phase is insensitive to electric field.

To gain further insight into the electric field effect, we perform a detailed study of the gate dependent resistance under isothermal conditions. Figure 3a shows the resistance at 115 K as the electric field is swept between +1.8 MV/cm and -1.8 MV/cm. Consistent with the shift in  $T_V$  (inset Fig. 2b), the resistance increases for both positive and negative electric fields and the effect is slightly larger for negative electric fields. To quantify the symmetry of the electric field effect, we separate the change in resistance  $\Delta R(E) = R(E) - R(0)$  into a symmetric part  $\Delta R_S(E) = [\Delta R(E) + \Delta R(-E)]/2$  (Fig. 3b) and anti-symmetric part  $\Delta R_A(E) = [\Delta R(E) - \Delta R(-E)]/2$  (Fig. 3c). Comparing Fig. 3b and 3c, the symmetric part is up to 11 times larger than the anti-symmetric part. Because the change in carrier concentration is proportional to  $E$  (i.e. anti-symmetric), the small contribution of  $\Delta R_A$  indicates that electric field control of the Verwey transition is not driven by a carrier concentration effect. Instead, a symmetric effect can be driven by other interactions with the electric field. The presence of an electric field will induce electric polarization given by  $P = \chi_e E = (\kappa - 1)\epsilon_0 E$ , where  $\chi_e$  is the electric susceptibility,  $\epsilon_0$  is the permittivity of free space, and  $\kappa$  is the relative dielectric constant of  $\text{Fe}_3\text{O}_4$ . The induced polarization will produce an energy contribution  $U = -\frac{1}{2}(PE) = -\frac{1}{2}(\kappa - 1)\epsilon_0 E^2$  that is symmetric in  $E$ . In addition, as  $\text{Fe}_3\text{O}_4$  undergoes the Verwey transition, the dielectric constant changes sharply with  $\kappa$  being larger for the insulating state than for the metallic state ( $\kappa_{ins} > \kappa_{metal}$ ) [33]. Thus, energy is lower for the insulating state than for the metallic state, which stabilizes the low temperature insulating state and causes  $T_V$  to increase. Therefore, this provides a macroscopic explanation for an electric field effect that is symmetric in  $E$  and produces an increase in  $T_V$ , consistent with experimental results. Further theoretical work is needed, including a microscopic model that can provide an explanation for the magnitude of the effect. In addition, a contribution from electric field induced strain could generate this symmetry and should also be investigated

[34].

Since the Verwey transition in  $\text{Fe}_3\text{O}_4$  is a correlated phase transition that couples both the charge and magnetic properties, it should be possible to tune magnetic properties with applied electric field. Figure 4a shows MOKE hysteresis loops measured at 113 K with applied electric field of 0 MV/cm (black) and -1.8 MV/cm (red). The absolute magnetization is determined by SQUID measurements (right axis of Figure 4a). An electric field of -1.8 MV/cm causes a decrease in the saturation magnetization of 18%. Figure 4b displays the saturation magnetization as the electric field is swept between +1.8 MV/cm and -1.8 MV/cm. With the application of either positive or negative field, the magnetization decreases with a slightly stronger effect for negative fields. The magnetoelectric behavior is generated because the magnetization has strong temperature dependence below  $T_V$  (Figure 1d). When electric field is applied, the increase of  $T_V$  causes magnetization  $M$  to decrease because  $dM/dT$  is positive at  $T = 113$  K; the intuitive picture is that the  $M$  vs  $T$  curve of Fig. 1d shifts toward higher temperature as  $T_V$  increases. Thus, the decrease of magnetization for both positive and negative fields (with slightly stronger effect for negative fields) is consistent with the electric field dependence of  $T_V$  (Fig. 2b inset) and resistance (Fig. 3). The change in magnetization as a function of electric field is quantified by a magnetoelectric coefficient,  $\alpha_{ME} = |\Delta M/\Delta E|$ , where  $\Delta M$  is the change in magnetization and  $\Delta E$  is the change in electric field. Comparing the values at  $E = 0$  MV/cm and  $E = -1.8$  MV/cm yields a value of  $\alpha_{ME} = 585 \pm 39$  pT m/V. Although at low temperatures, this is quite a large magnetoelectric coefficient compared to other materials [32]. These results are compelling because they demonstrate a new method for generating magnetoelectric effects by controlling a correlated phase transition.

In conclusion, we have demonstrated the electric field control of the Verwey transition in  $\text{Fe}_3\text{O}_4$  thin films. An electric field stabilizes the charge-ordered insulating state causing the Verwey transition temperature to increase. By manipulating a correlated phase transition that combines both charge and magnetic transitions, we realize a novel magnetoelectric effect.

We acknowledge K. M. McCreary and P. M. Odenthal for their assistance. This material is based on research sponsored by DARPA/Defense Microelectronics Activity (DMEA) under agreement number H94003-10-2-1004. We acknowledge Youli Li at the UCSB MRL Central Facilities (NSF Award No. DMR 1121053) for technical assistance with x-ray diffraction

measurements and discussion.

---

\* roland.kawakami@ucr.edu

- [1] C. H. Ahn, J.-M. Triscone, and J. M. Mannhart, *Nature* **424**, 1015 (2003).
- [2] A. Asamitsu, Y. Tomioka, H. Kuwahara, and Y. Tokura, *Nature* **388**, 50 (1997).
- [3] S. Lee, A. Fursina, J. T. Mayo, C. T. Yavuz, V. L. Colvin, R. G. S. Sofin, I. V. Shvets, and D. Natelson, *Nature Mater.* **7**, 130 (2008).
- [4] T. Lottermoser, T. Lonkai, U. Amann, D. Hohlwein, J. Ihringer, and M. Fiebig, *Nature* **430**, 541 (2004).
- [5] H. Zheng, J. Wang, S. E. Lofland, Z. Ma, L. Mohaddes-Ardabili, T. Zhao, L. Salamanca-Riba, S. R. Shinde, S. B. Ogale, F. Bai, D. Viehland, Y. Jia, D. G. Schlom, M. Wuttig, A. Roytburd, and R. Ramesh, *Science* **303**, 661 (2004).
- [6] E. J. W. Verwey, *Nature* **144**, 327 (1939).
- [7] E. J. W. Verwey and P. W. Haayman, *Physica* **8**, 979 (1941).
- [8] F. Walz, *J. Phys.: Condens. Matter* **14**, R285 (2002).
- [9] V. A. M. Brabers, F. Walz, and H. Kronmuller, *Phys. Rev. B* **58**, 14163 (1998).
- [10] Y. Ding, D. Haskel, S. G. Ovchinnikov, Y.-C. Tseng, Y. S. Orlov, J. C. Lang, and H.-K. Mao, *Phys. Rev. Lett.* **100**, 045508 (2008).
- [11] J. Garcia, G. Subias, J. Herrero-Martin, J. Blasco, V. Cuartero, M. C. Sanchez, C. Mazzoli, and F. Yakhou, *Phys. Rev. Lett.* **102**, 176405 (2009).
- [12] D. J. Huang, H. J. Lin, J. Okamoto, K. S. Chao, H. T. Jeng, G. Y. Guo, C. H. Hsu, C. M. Huang, D. C. Ling, W. B. Wu, C. S. Yang, and C. T. Chen, *Phys. Rev. Lett.* **96**, 096401 (2006).
- [13] J. E. Lorenzo, C. Mazzoli, N. Jaouen, C. Detlefs, D. Mannix, S. Grenier, Y. Joly, and C. Marin, *Phys. Rev. Lett.* **101**, 226401 (2008).
- [14] G. K. Rozenberg, M. P. Pasternak, W. M. Xu, Y. Amiel, M. Hanfland, M. Amboage, R. D. Taylor, and R. Jeanloz, *Phys. Rev. Lett.* **96**, 045705 (2006).
- [15] M. S. Senn, J. P. Wright, and J. P. Attfield, *Nature* **481**, 173 (2011).
- [16] F. Zhou and G. Ceder, *Phys. Rev. B* **81**, 205113 (2010).
- [17] M. Alexe, M. Ziese, D. Hesse, P. Esquinazi, K. Yamauchi, T. Fukushima, S. Picozzi, and

- U. Gosele, *Adv. Mater.* **21**, 4452 (2009).
- [18] J. van den Brink and D. I. Khomskii, *J. Phys.: Condens. Matter* **20**, 434217 (2008).
- [19] G. T. Rado and J. M. Ferrari, *Phys. Rev. B* **15**, 290 (1977).
- [20] K. Kato, S. Iida, K. Yanai, and K. Mizushima, *J. Magn. Magn. Mater.* **31-34**, 783 (1983).
- [21] Y. Miyamoto, S. Ishihara, T. Hirano, M. Takada, and N. Suzuki, *Solid State Comm.* **89**, 51 (1994).
- [22] Z. Zhang and S. Satpathy, *Phys. Rev. B* **44**, 13319 (1991).
- [23] P. Seneor, A. Fert, J.-L. Maurice, F. Montaigne, F. Petroff, and A. Vaures, *Appl. Phys. Lett.* **74**, 4017 (1999).
- [24] Y. Li, W. Han, A. G. Swartz, K. Pi, J. J. I. Wong, S. Mack, D. D. Awschalom, and R. K. Kawakami, *Phys. Rev. Lett.* **105**, 167203 (2010).
- [25] W. Eerenstein, T. T. M. Palstra, T. Hibma, and S. Celotto, *Phys. Rev. B* **66**, 201101(R) (2002).
- [26] F. Wang, C.-H. Li, T. Zou, L. Yi, and Y. Sun, *J. Phys.: Condens. Matter* **22**, 496001 (2010).
- [27] C. A. F. Vaz, J. Hoffman, Y. Segal, J. W. Reiner, R. D. Grober, Z. Zhang, C. H. Ahn, and F. J. Walker, *Phys. Rev. Lett.* **104**, 127202 (2010), pRL.
- [28] J. Ryu, A. V. Carazo, K. Uchino, and H.-E. Kim, *Jpn. J. Appl. Phys.* **40**, 4948 (2001).
- [29] J. Ryu, S. Priya, K. Uchino, and H.-E. Kim, *J. Electroceram.* **8**, 107 (2002).
- [30] L. Yan, Z. Wang, Z. Xing, and J. Li, *J. Appl. Phys.* **107**, 064106 (2010).
- [31] J. J. I. Wong, L. Ramirez, A. G. Swartz, A. Hoff, W. Han, Y. Li, and R. K. Kawakami, *Phys. Rev. B* **81**, 094406 (2010).
- [32] See Supplemental Material at <http://>.
- [33] A. Pimenov, S. Tachos, T. Rudolf, A. Loidl, D. Schrupp, M. Sing, R. Claessen, and V. A. M. Brabers, *Phys. Rev. B* **72**, 035131 (2005).
- [34] Y. Nagasawa, M. Kosaka, S. Katano, N. Mori, S. Tado, and Y. Uwatoko, *J. Phys. Soc. Jpn.* **76**, 110 (2007).

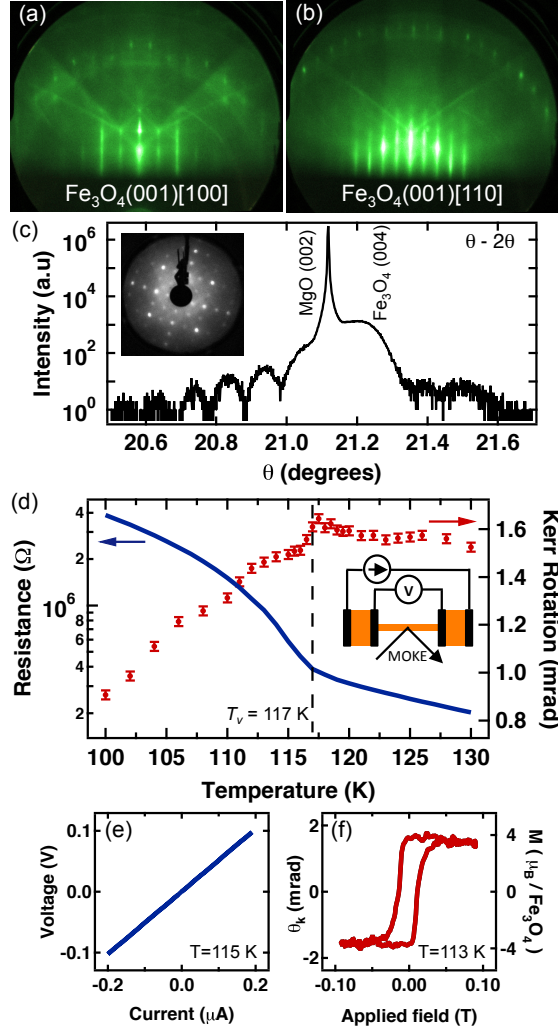


FIG. 1. Characterization of  $\text{Fe}_3\text{O}_4$  thin films. (a) and (b) are RHEED patterns for 50 nm  $\text{Fe}_3\text{O}_4$  on  $\text{MgO}(001)$  along the  $[100]$  and  $[110]$  in-plane directions, respectively. (c) HRXRD  $\theta - 2\theta$  scans measured around the location of the  $\text{MgO}(002)$  peak with Kiessig fringes. Inset: LEED pattern with incident energy of 160 eV. (d) Temperature dependence of resistance measured by four-point probe (blue) and magnetization measured by MOKE (red). The vertical dashed line indicates the Verwey transition. Inset: geometry for the resistance and magnetization measurements. (e)  $I$ - $V$  curve for  $\text{Fe}_3\text{O}_4$  channel at 115 K. (f) MOKE hysteresis loop for  $\text{Fe}_3\text{O}_4$  at 113 K. The right axis shows absolute magnetization based on SQUID measurements on corresponding samples.

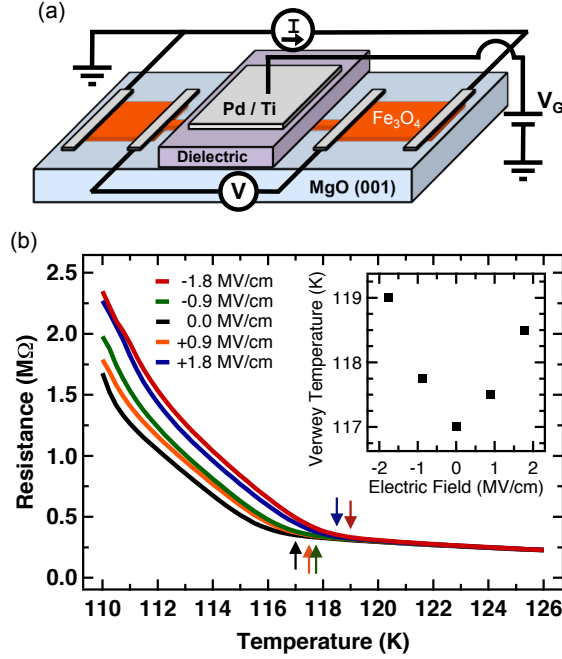


FIG. 2. Electrical gating of Fe<sub>3</sub>O<sub>4</sub> and manipulation of the Verwey transition. (a) A schematic of the sample device structure. The dielectric layer consists of PMMA(900 nm)/Al<sub>2</sub>O<sub>3</sub>(50 nm)/MgO(10 nm). Positive electric field corresponds to the application of positive voltage to the top gate electrode. (b) Temperature dependence of resistance for applied electric fields of +1.8 MV/cm (blue), +0.9 MV/cm (orange), 0 MV/cm (black; from Fig. 1d), -0.9 MV/cm (green), -1.8 MV/cm (red). The arrows show  $T_V$  for each electric field, which is summarized in the inset.

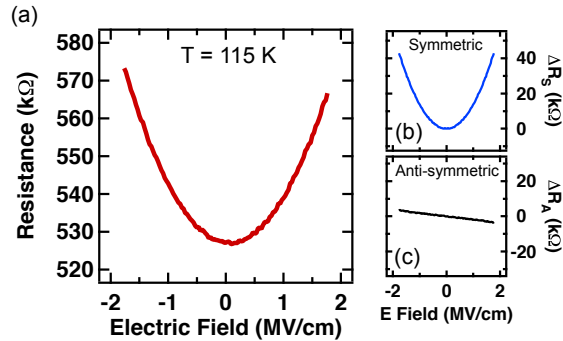


FIG. 3. Electrostatic gate dependence of resistance. (a) Gate dependent resistance for Fe<sub>3</sub>O<sub>4</sub> at a temperature of 115 K. (b) and (c) show the symmetric and anti-symmetric components of the gate dependent resistance change, respectively.

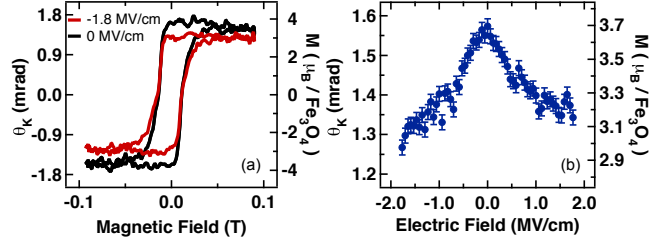


FIG. 4. Electrostatic gate dependence of magnetization. (a) MOKE loops measured at 113 K with applied electric fields of 0 MV/cm (black) and -1.8 MV/cm (red), showing a decrease in magnetization with the application of an electric field. (b) Magnetization as a function of electric field, demonstrating a magnetoelectric effect induced by electric field control of the Verwey transition.